Modeling and Identification of an Electric Vehicle Braking System: Thermal and Tribology Phenomena Assessment

2020-01-1094

Modeling and Identification of an Electric Vehicle Braking System: Thermal and Tribology Phenomena Assessment

Thomas D'hondt, Bart Forrier and Mathieu Sarrazin
Siemens Industry Software NV, Belgium

Tommaso Favilli, Luca Pugi, Lorenzo Berzi, Riccardo Viviani and Marco Pierini
Università degli Studi di Firenze, Italy

Abstract

A rapidly shifting market and increasingly stringent environmental regulations require the automotive industry to produce more efficient low-emission Eletric Vehicles (EVs). Regenerative braking has proven to be a major contributor to both objectives, enabling the charging of the batteries during braking and a reduction of the load and wear of the brake pads. The optimal sizing of such systems requires the availability of good simulation models to improve their performance and reliability at all stages of the vehicle design. This enables the designer to study both the integration of the braking system with the full vehicle equipment and the interactions between electrical and mechanical braking strategies. This paper presents a generic simulation framework for the identification of thermal and wear behaviour of a mechanical braking system, based on a lumped parameter approach. The thermal behaviour of the system is coupled back to the friction coefficient between the pad and the disk to assess its effect on braking performance. Additionally, the effect of wear and temperature on the generation of airborne particles is investigated. Subsequently, experimental data collected on a real EV is used to validate and tune the previously described simulation model, following a proposed validation procedure. The instrumentation method and challenges, as well as the experimental procedure used to collect the data on a chassis dynamometer and in real-world driving conditions, are described. Finally, simulation results for different driving scenarios are used to compare virtual and experimental results.

Introduction

The transition from Internal Combustion Engine (ICE) vehicles to electric ones appears to be a feasible solution to reduce the environmental impact of mobility [1], while improving performance and comfort at the same time [2, 3]. Therefore, EVs have steadily grown in market share over the last years and start to become an industrial reality [4]. However, safety and driving range remain open issues, requiring thorough investigations by the Original Equipment Manufacturer (OEM) during the entire development and validation cycle of the EV. Solving those issues will be a major requirement for the widespread adoption of EVs in the coming years.

The availability of regenerative braking in EVs can lead to many advantages, ranging from an overall increase in efficiency to a reduction in brake wear and maintenance costs [5, 6, 7, 8]. However, it is currently unable to provide sufficient braking performance by itself in every operating condition [9]. Therefore, appropriate integration of regenerative and mechanical braking is required. The usage of simulation models throughout the development process can help engineers with the sizing, integration and safety validation issues associated with such complex braking strategies.

In order to simulate the behaviour of a vehicle with sufficient fidelity, both accurate models and appropriate parameter calibration methods are required. Therefore, the present paper proposes an enhanced simulation model for the braking system of the SimRod, an EV prototyping platform (Figure 1). The authors focus on the assessment of the thermal and tribological aspects of its mechanical

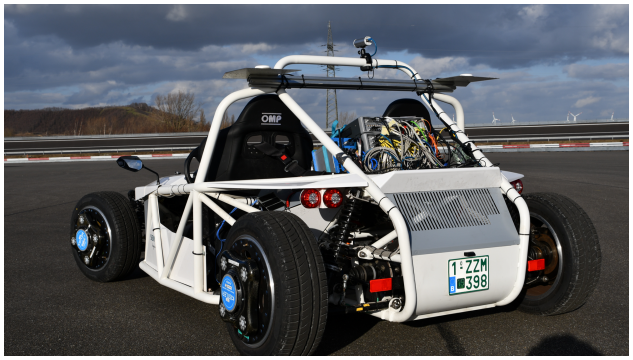

Figure 1: SimRod electric test vehicle

braking system. This includes the interaction between the pad interface temperature and the available friction coefficient, to define its influence on the vehicle braking performances. Additionally, the wear of the brake pad is simulated, which is one of the major sources of fine particle emissions in EVs [10]. Finally, an approach for the identification of accurate model parameters is proposed and evaluated using data collected on a chassis dynamometer and in real driving conditions.

The paper is organised as follows: firstly, the modelling and the simulation process are described. Then, the experimental instrumentation and measurement process are presented, followed by the identification methodology and calibration procedure. Finally, some conclusions on the results and future developments are considered.

Simulation of braking systems

The SimRod braking system is represented in Figure 2. It consists of a TT layout, where one master cylinder controls both front brakes and the other cylinder controls the rear ones. This allows for good control of the front-rear brake balance. Both front and rear brakes use disks, but only the front ones have cooling vanes.

The corresponding brake plant simulation model is divided into multiple sub-models, each representing a specific component of the system or a physical phenomenon (Figure 3). The hydraulics model reproduces

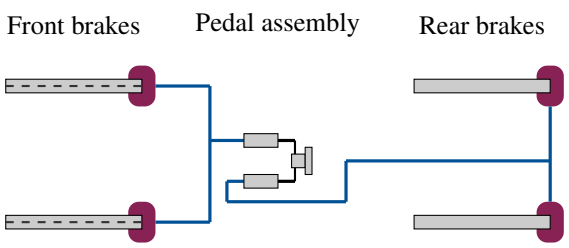

Figure 2: Overview of the SimRod braking plant

the effect of a driver input u_b, such as the pedal displacement, on the pressure $p^{\mathrm{i}}_{\mathrm{cal}}$ in each calliper pistons, where $\mathrm{i} \in \{\mathrm{RL}, \mathrm{RR}, \mathrm{FL}, \mathrm{FR}\}$. This includes the effects of the pedal, master cylinder, brake booster, hydraulic modulator, hydraulic lines and piston displacement. The demanded piston pressure $p^{\mathrm{i}}_{\mathrm{cal}}$ is then transformed into a torque τ^{i} due to the friction between the pad and the braking disk. Together, the braking torques on each wheel affect the dynamic behaviour of the vehicle, which is here summarised by the vehicle longitudinal speed $\dot{x}$ and acceleration $\ddot{x}$. The friction torque τ^{i}, speed $\dot{x}$ and ambient temperature are inputs to the thermal model of the plant. It computes the temperature of different components of the brake system, including the disk-pad interface temperature $T^{\mathrm{i}}_{\mathrm{if}}$. The latter is fed back to the torque sub-model since the friction coefficient between the pad and the disk is a function of this temperature. Finally, both the friction torque τ^{i} and the interface temperature $T^{\mathrm{i}}_{\mathrm{if}}$ affect the wear of the braking pad.

In the present paper, the hydraulic model is not further studied. This limitation is by-passed by measuring directly the pressure $p^{\mathrm{i}}_{\mathrm{cal}}$ on the real vehicle calliper, which can then be fed as an input to the simulation model for its validation.

Torque computation

The friction torque τ^{i} generated at a single wheel is given by (1).

$$\tau^{\mathrm{i}} = 2\mu(T^{\mathrm{i}}_{\mathrm{if}})p^{\mathrm{i}}_{\mathrm{cal}}A^{\mathrm{i}}_{\mathrm{pist}}\bar{r}^{\mathrm{i}} \tag{1}$$

The pad-disk friction coefficient μ is assumed to be a function of pad interface temperature $T^{\mathrm{i}}_{\mathrm{if}}$. A corresponding friction force is generated due to the normal force applied by a single pad on the disk. This force is computed using the calliper pressure $p^{\mathrm{i}}_{\mathrm{cal}}$ and the area of the piston $A^{\mathrm{i}}_{\mathrm{pist}}$. Finally, this force is transformed into an equivalent torque, assuming an average radius $\bar{r}^{\mathrm{i}}$ of application. Due to the floating calliper configuration, this force is applied by both pads on the two sides of the disk, hence the factor two.

Thermal behaviour

The thermal behaviour of the braking system is modelled using an equivalent electrical circuit [11]. This circuit is composed of multiple basic elements (Figure 4):

- The temperature source (Figure 4a) imposes a constant temperature gradient $\Delta T = T_s$ across its terminals. It can be used for instance to define the

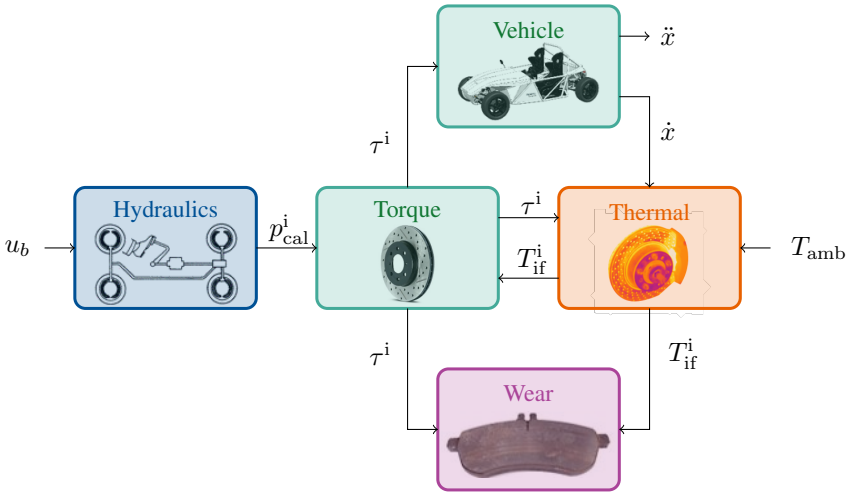

Figure 3: Decomposition of the braking plant simulation model into different sub-models

ambient temperature T_{amb} with respect to the thermal reference.

- The heat rate source (Figure 4b) imposes a constant heat rate $\dot{Q} = \dot{Q}_s$ through its circuit branch. A common application is the modelling of the generated heat at the interface between the braking pad and the disk.
- The thermal resistance (Figure 4c) models the heat transfer between two bodies at different temperatures $\Delta T = R\dot{Q}$. This element can be used to model both conduction and convection phenomena.
- The thermal mass (Figure 4d) represents the thermal inertia of a body: its ability to store thermal energy. In the present model, it is always referred to the thermal reference on one of its terminals. Therefore, it imposes the temperature of the considered body on its other terminal as a function of the rate of heat $\dot{Q}$ entering the body $C\frac{d\Delta T}{dt} = C\frac{dT}{dt} = \dot{Q}$.

The model presented in this paper focuses on the thermal behaviour of the calliper assembly and the non-vaned braking disk of one of the rear brakes (Figure 5). The interface region between the disk and one of the braking pads, indicated in red, is represented by a heat source $\dot{Q}^{\mathrm{i}}$ and a small equivalent thermal mass $C^{\mathrm{i}}_{\mathrm{if}}$. The latter represents the local mass around the pad-disk interface which heats up very quickly during braking manoeuvres and whose temperature is given by $T^{\mathrm{i}}_{\mathrm{if}}$. The resulting heat is then further propagated, either towards the disk or towards the pad. The disk thermal capacity and resistance are given by $C^{\mathrm{i}}_{\mathrm{disk}}$ and $R^{\mathrm{i}}_{\mathrm{disk}}$, respectively. The hub temperature $T^{\mathrm{i}}_{\mathrm{hub}}$ is then defined by the hub thermal resistance $R^{\mathrm{i}}_{\mathrm{hub}}$ and capacitance $C^{\mathrm{i}}_{\mathrm{hub}}$. On the other side of the model, the heat generated during braking is propagated to the pad, the piston, the calliper and the braking fluid. Their respective thermal resistance and capacitances are indicated in Figure 5.

The interface convection thermal resistances $R^{\mathrm{i}}_{\mathrm{pad,\ conv}}$ and $R^{\mathrm{i}}_{\mathrm{disk,\ conv}}$ have both been scheduled as a linear function of vehicle speed to account for the increase in cooling at higher speeds. However, when the pressure $p^{\mathrm{i}}_{\mathrm{cal}}$ is greater than zero, the pad-to-air thermal resistance $R^{\mathrm{i}}_{\mathrm{pad,\ conv}}$ is very high as most of the pad surface is in contact with the disk and no longer with air. This has been modelled by stepping $R^{\mathrm{i}}_{\mathrm{pad,\ conv}}$ to an arbitrarily high value when $p^{\mathrm{i}}_{\mathrm{cal}} > 0$.

Finally, it is assumed that all the energy dissipated by the friction between the pad and the disk is converted into heat. Supposing that this heat is divided equally amongst both brake pads, symmetrically along the half-plane of the disk, the injected heat into the thermal model of the

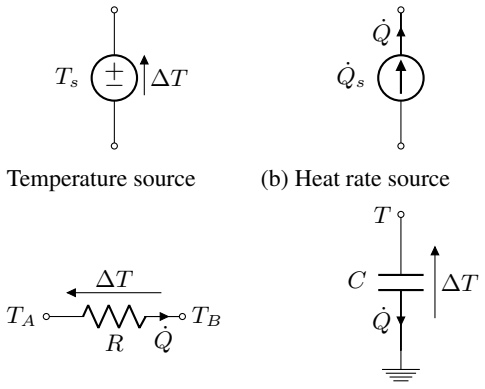

(a) Temperature source (b) Heat rate source

(c) Thermal resistance (d) Thermal mass

Figure 4: Equivalent thermal modelling of the brake system using basic elements

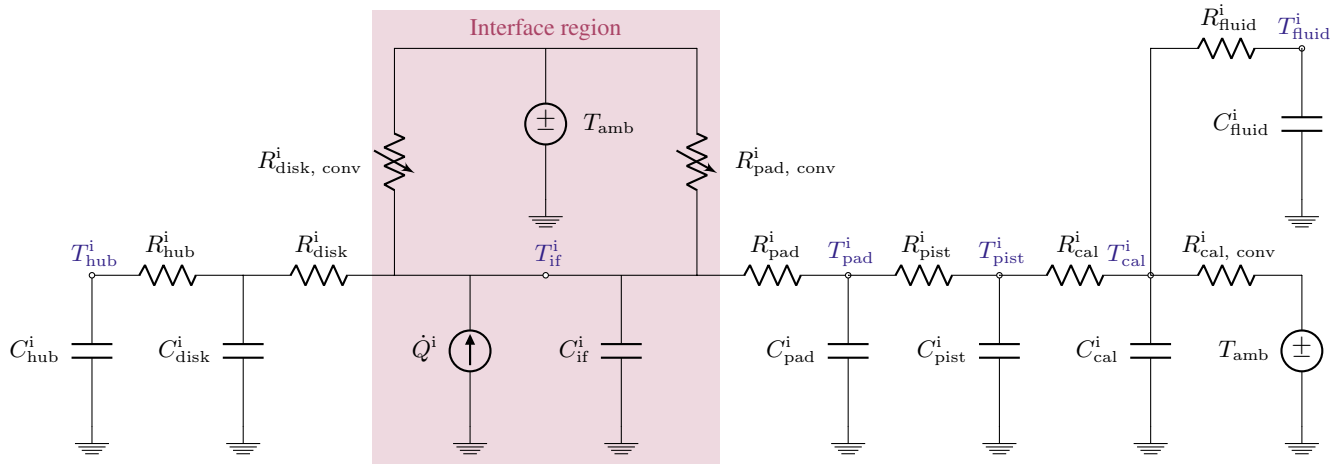

Figure 5: Equivalent thermal RC network for a single rear brake pad of the vehicle. Temperature measurement points are indicated with dots.

braking system is given by (2).

$$\dot{Q}^{\text{i}} = \frac{|\tau^{\text{i}}\omega^{\text{i}}|}{2} \tag{2}$$

A similar exercise can be done for the simulation of the front brakes of the car. The major change with respect to the proposed model for the rear brakes, besides the difference in overall geometry, is that the front disk is vaned on the SimRod. This should improve the convection cooling of the system and can be considered using an adapted speed-varying thermal resistance.

Wear behaviour

The friction between a braking pad and the disk results in the wear of both components. In this paper, the wear of pad material is modelled according to a generalized form of Archard's law, which can be expressed in cylindrical coordinates as [12, 13]:

$$\frac{dh}{d\theta} = kpr \tag{3}$$

In (3), h is the worn height of a pad, k is the associated dimensional wear coefficient, p is the contact pressure between the disk and the pad and r is the radius at which the wear occurs. The dimensional wear coefficient k is the ratio between Archard's dimensionless wear coefficient and the hardness of the softer contact surface. After multiplying both sides by $\frac{d\theta}{dt}$, this equation can be rewritten as:

$$\frac{dh}{dt} = kpr\omega \tag{4}$$

Finally, it is applied to a single pad inside one of the brake callipers of the car. It is furthermore assumed that the wear occurs at a constant average radius of $r = \bar{r}^{\text{i}}$. Therefore, integrating from the start of the experiment time t_0 until the end of the experiment t_f:

$$\bar{h}^{\text{i}} = \int_{t_0}^{t_f} kp^i\bar{r}^{\text{i}}\omega^{\text{i}}\, dt \tag{5}$$

In (5), $\bar{h}^{\text{i}}$ is the worn height of a single pad, $p^i = p^{\text{i}}_{\text{cal}}\frac{A^{\text{i}}_{\text{pist}}}{A^{\text{i}}_{\text{pad}}}$ the contact pressure between the disk and the pad, $\bar{r}^{\text{i}}$ the mean braking radius and ω^{i} the angular speed of the disk.

As shown in [14], the dimensional wear coefficient k is a function of the interface temperature T^{i}_{if}. The values used in this paper were obtained by matching the experimental and predicted worn masses for a pad of the vehicle (Figure 6). This curve is a bi-linear approximation of the fading phenomenon and represents a wear increase at high temperature due to the degradation of the mechanical properties of the material.

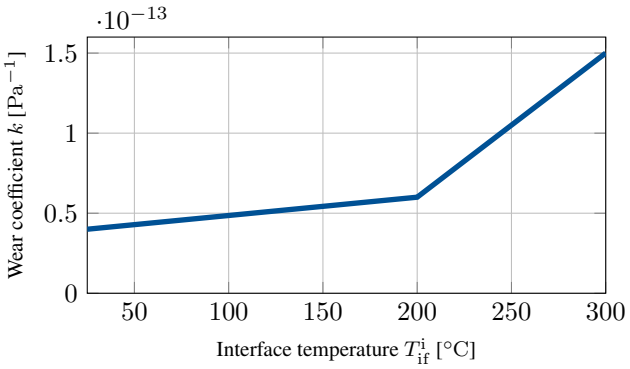

Figure 6: Pad wear coefficient k as a function of the pad temperature

The worn mass $m_{\mathrm{f}}^{\mathrm{i}} = \rho_{\mathrm{pad}} \bar{h}^{\mathrm{i}} A_{\mathrm{pad}}^{\mathrm{i}}$ per pad is obtained assuming that the pads wear uniformly across their surface. In this equation, ρ_{pad} is the density of the pad material and $A_{\mathrm{pad}}^{\mathrm{i}}$ its surface area. The resulting mass of emitted airborne particles in the environment $m_{\mathrm{PM}}^{\mathrm{i}}$ corresponds on average to 35% of the total worn mass $m_{\mathrm{f}}^{\mathrm{i}}$ [15]. Those particles can then be divided into two main groups, according to their size:

$$\begin{aligned} \mathrm{PM}_{10}^{\mathrm{i}} &= 0.86\, m_{\mathrm{PM}}^{\mathrm{i}} \\ \mathrm{PM}_{2.5}^{\mathrm{i}} &= 0.63\, m_{\mathrm{PM}}^{\mathrm{i}} \end{aligned} \tag{6}$$

The wear on the four callipers should finally be summed, considering two pads per calliper, to obtain the total worn mass for the entire car.

$$\mathrm{PM}_{10}^{\mathrm{tot}} = 2 \sum_i \mathrm{PM}_{10}^{\mathrm{i}} \qquad \mathrm{PM}_{2.5}^{\mathrm{tot}} = 2 \sum_i \mathrm{PM}_{2.5}^{\mathrm{i}} \tag{7}$$

Experimental validation

System instrumentation

The braking system of the SimRod has been instrumented with several thermal sensors for the identification of the simulation model parameters (Figure 7). They were laid out on the rear-left brake, following the different measurement points indicated in the equivalent thermal RC network (Figure 5). Where appropriate, regular K-type thermocouples were used due to their lower cost and wide availability (Figure 7a, Figure 7e and Figure 7f). Both a rubbing thermocouple (Figure 7b) and a 16 points 1D infrared sensor (Figure 7c) were used to measure the disk interface temperature. Additionally, a pad thermocouple was used to measure the internal temperature in the pad at a known distance from the surface (Figure 7d). This sensor was mounted using a specific epoxy as to not affect the mechanical integrity and the thermal properties of the braking pad during the test campaign. Finally, the ambient temperature is measured using an external sensor.

The two types of sensors used to measure the interface temperature were chosen due to their complementary characteristics. Indeed, the rubbing thermocouple will wear over time, measures only at a single radius of the disk and has greater thermal inertia and, hence, a lower bandwidth. On the other hand, the infrared sensor measures 16 radii simultaneously without direct contact with the disk, giving us a better idea on the distribution of the temperature over the disk surface. However, the low emissivity of the brake disk makes the calibration of the sensor hard, without the reference provided by the rubbing thermocouple [16].

Other physical quantities were measured on the car during the tests, such as the pressure inside the braking system. The SimRod has a fully-split front and rear braking circuit with two independent master cylinders and no hydraulic modulator. Therefore, the pressure was measured at two points: next to the rear-left and next to the front-right callipers. The rotational speed of the rear wheels was acquired using an optical sensor and zebra tape mounted on the rear axle. GPS data was acquired during outdoor measurements. Finally, all of the data was collected using a multi-physical data acquisition system: the Simcenter SCADAS and Testlab.

Measurement scenarios

The identification measurements took place in the controlled environment of a chassis dynamometer (Figure 8). The braking pedal was fixed at a constant displacement using a mechanical assembly installed on the mounting

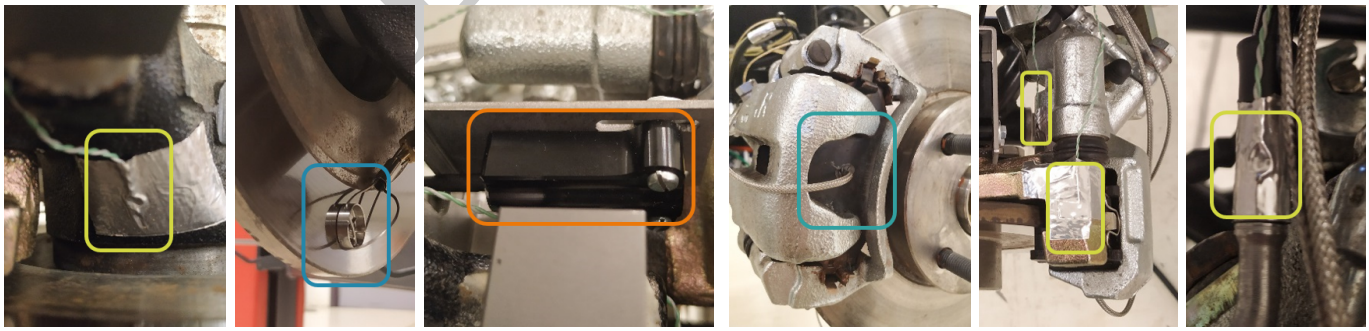

(a) Hub thermocouple $T_{\mathrm{hub}}^{\mathrm{RL}}$ (b) Rubbing thermocouple $T_{\mathrm{if}}^{\mathrm{RL}}$ (c) Disk infrared sensor $T_{\mathrm{if}}^{\mathrm{RL}}$ (d) Pad interior thermocouple $T_{\mathrm{pad}}^{\mathrm{RL}}$ (e) Calliper $T_{\mathrm{cal}}^{\mathrm{RL}}$ and piston $T_{\mathrm{pist}}^{\mathrm{RL}}$ sensors (f) Fluid thermocouple $T_{\mathrm{fluid}}^{\mathrm{RL}}$

Figure 7: Thermal sensors instrumented on the left-rear brake of the SimRod

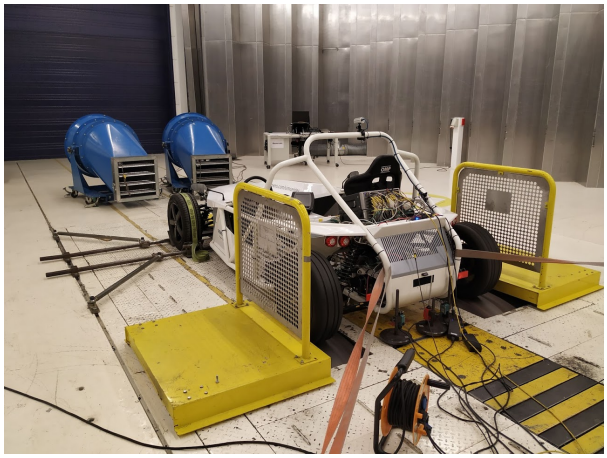

(a) SimRod installed on the chassis dynamometer during the rear-left brake testing

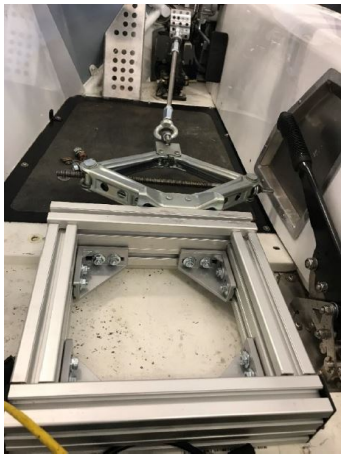

(b) Frame attached to the seat mounting points

(c) Rod keeping the pedal at a constant displacement

Figure 8: Chassis dynamometer experimental setup

points of the seat for rigidity. Meanwhile, the rear wheels of the car were spinning at a constant speed imposed by the testbed. Different measurement runs were recorded considering several speeds and pedal displacements (Table 1).

One should note that the constant displacement imposed to the pedal means that the pressure inside the hydraulic circuit was varying during the experiments. Indeed, the heat generated by the braking action partly propagates to the braking fluid, whose subsequent expansions results in a gradual increase of the pressure in the system. This in turns increases the braking torque and, therefore, the generation of heat. It was consequently decided to stop the measurements when reaching a safe threshold of interface temperature since no thermal equilibrium was observed. This was also required considering the electrical nature of the car and the fire hazards related to its batteries.

Then, real-world validation tests were performed on a private road using the same instrumentation. Successive run-ups and brake manoeuvres were executed repeatedly to heat up the system. Wheel lock-up conditions were avoided during those experimental runs.

Finally, new braking pads were installed on the car before the first test on the chassis dynamometer. Their weight was measured before and after the experimental runs listed in Table 1 and the real-world tests for the evaluation of the wear model.

Table 1: Experimental runs evaluated on the chassis dynamometer

Run	$p_{\mathrm{c},0}^{\mathrm{RL}}$ [bar]	$\dot{x}$ [km h^{-1}]
1	8	10
2	7	5
3	2	30
4	4	50

Identification methodology

Friction coefficient identification

One of the important parameters in the simulation model is the friction coefficient μ between the pad and the disk, as it directly links the braking pressure and the resulting torque. On the dynamometer, the dissipated power P_{br} is obtained from the product between the rotational speed ω^{i} and the torque τ^{i} of the rear wheels:

$$\begin{aligned} P_{\mathrm{br}} &= \omega^{\mathrm{RL}}\tau^{\mathrm{RL}} + \omega^{\mathrm{RR}}\tau^{\mathrm{RR}} \\ &= 2\omega^{\mathrm{RL}}\tau^{\mathrm{RL}} \end{aligned} \tag{8}$$

In the last equation, it is assumed that the left and rear side of the car behave equally on the dynamometer. Then, substituting with (1):

$$\mu(T_{\mathrm{if}}^{\mathrm{RL}}) = \frac{P_{\mathrm{br}}}{2\omega^{\mathrm{RL}} p_{\mathrm{cal}}^{\mathrm{RL}} A_{\mathrm{pist}}^{\mathrm{RL}} \bar{r}^{\mathrm{RL}}} \tag{9}$$

All values on the right-hand side of (9) are known a priori or measured directly on the testbed. Hence, the friction coefficient μ can be computed for all experimental runs as a function of $T_{\mathrm{if}}^{\mathrm{i}}$. Subsequently, this data was filtered to obtain smoother curves using a zero-phase filter. Finally, those smoothed curves were arithmetically averaged for each interface temperature $T_{\mathrm{if}}^{\mathrm{i}}$ to obtain a unique friction curve $\mu(\,T_{\mathrm{if}}^{\mathrm{i}})$ for use in the simulation model.

Thermal properties identification

Initial approximate values for the thermal capacitances were computed based on the weight of the individual components when accessible. Alternatively, the detailed 3D geometry of the car was used in a CAD software to obtain their volume, which was then used to compute the corresponding mass using their density. Combined with the specific heat of the material, an approximated thermal capacitance can be computed. For the thermal resistances representing conduction and convection, initial values were used from [17] when available.

The final tuning of the different thermal parameters was done manually. Therefore, the dissipated heat at the disc-pad interface was computed based on the acquired data for a all measurement runs. It was then imposed as an input to the simulation model and the resulting predicted and measured temperatures were compared. Subsequently, the closest parameters to the interface were tuned to find a good correspondence between experimental and simulated temperatures. Gradually, parameters further away from the interface were tuned to obtain an overall good match. An optimization-based approach could be studied in future work to automate this process.

Results discussion

Friction coefficient results

The friction coefficient μ was evaluated for the different runs listed in Table 1 using (9). The results are plotted as a function of the interface temperature $T_{\mathrm{if}}^{\mathrm{RL}}$ in Figure 9. It is observed that for $T_{\mathrm{if}}^{\mathrm{RL}} \leq 100\,^{\circ}\mathrm{C}$, the friction coefficient μ tends to increase. For $100\,^{\circ}\mathrm{C} < T_{\mathrm{if}}^{\mathrm{RL}} \leq 200\,^{\circ}\mathrm{C}$, μ stays approximately constant and, finally, μ decreases again for higher temperatures. The overall trends of these curves, as well as their absolute value correspond to typical materials observed in the industry [17].

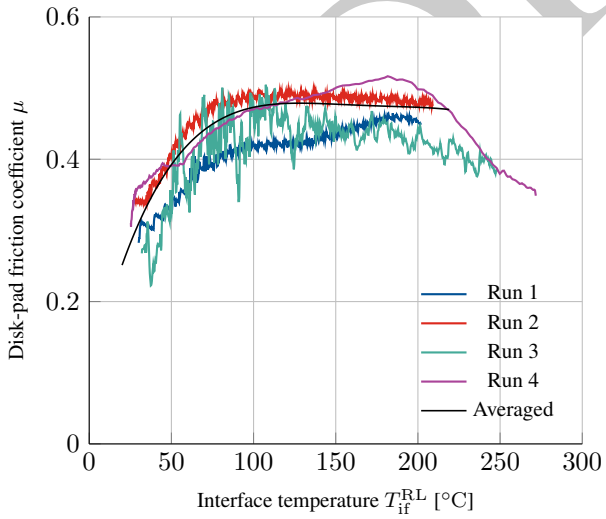

Figure 9: Estimated friction coefficient for the different measurement runs as a function of interface temperature $T_{\mathrm{if}}^{\mathrm{RL}}$

The experimental run 3 has higher noise compared to the other runs, which can be explained by a resonance of the mechanical assembly (between dynamometer & car). Indeed, some additional vibrations were directly visible on the car at that speed. Also, lower speed tests tend to have higher noise than other tests conducted at higher speed, as seen in runs 1 and 2. This can be justified by a slight misalignment on the disk or by its imperfect flatness. The rotational-dependency of this noise means that it tends to get filtered out by the system dynamics at higher speeds. All those sources of noise were filtered out as described in the methodology section of this paper.

The curve obtained by averaging all of this smoothed data is plotted in black in Figure 9 and was used as $\mu(\,T_{\mathrm{if}}^{\mathrm{i}})$ in the following simulations. The authors intend to further investigate the differences in measured μ across the different runs. One possible path forward is to also consider the dependency between μ and the contact pressure between the pad and disk. This could affect the physical properties of the micro-contact patches causing a variation in the macroscopic friction coefficient.

Thermal behaviour validation

After identifying the different thermal resistances and capacities of the system, the simulation model was executed on the different recorded runs for its validation. For this purpose, measured pressure and speed were imposed directly to the model and the thermal responses of the different braking system components were compared. In the following paragraphs, the results for run 3 are presented.

Firstly, a good match is observed between the measured and the predicted temperatures of the interface region and the piston (Figure 10a). During the first 1500 s of the experimental run, the temperature increases up to 200 °C. It was not possible to obtain a thermal steady-state due to the increase in pressure in the hydraulic lines linked to the expansion of the braking fluid. Therefore, the test was stopped manually at that time by turning-off shortly the chassis dynamometer. Subsequently, the operators retracted the brake pedal locking mechanism, before restarting the testbed with its initial speed. The short period during which the wheels are not rotating corresponds to the slow decrease in interface temperature

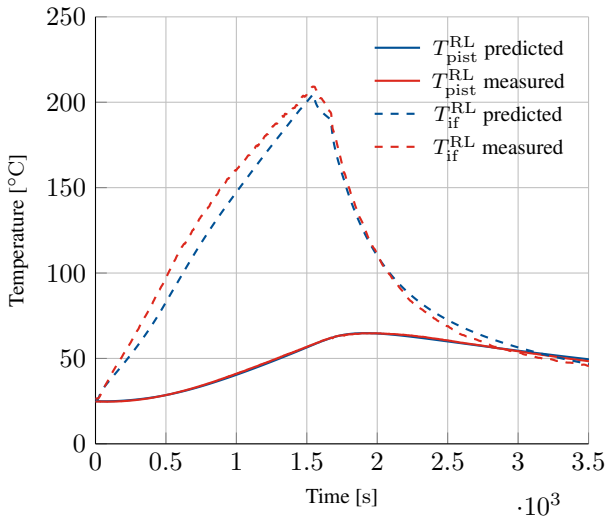

(a) Interface and piston temperatures

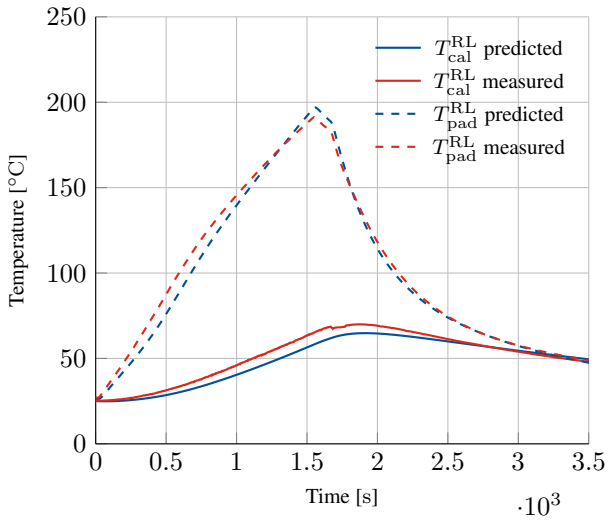

(b) Pad and calliper temperatures

Figure 10: Comparison between predicted and simulated temperatures for run 3

($1500\,\mathrm{s} \lessapprox t \lessapprox 1700\,\mathrm{s}$). Once the dynamometer is restarted, the decrease in temperature accelerates again thanks to the increased convection. It should be noted that a lag exists between the maximum interface and piston temperatures: while the former is already cooling down, the latter still heats up due to the thermal inertia of the interposed component. Similarly, a comparison between the pad and calliper temperatures is provided (Figure 10b).

Finally, the simulation model was used to predict the thermal behaviour of the braking system in a real-world driving scenario (Figure 11). During the first part of the experiment ($t \lessapprox 100\,\mathrm{s}$), the driver was quickly alternating between accelerating and braking manoeuvres, resulting in increasing temperatures. Afterwards, the car was stopped and the system was cooled, thanks to the convection with air, while the brake was still applied to keep the pad-disk contact. The measured pressure and GPS speed were used as inputs to the simulation model. A good match is observed between the predicted and the measured results.

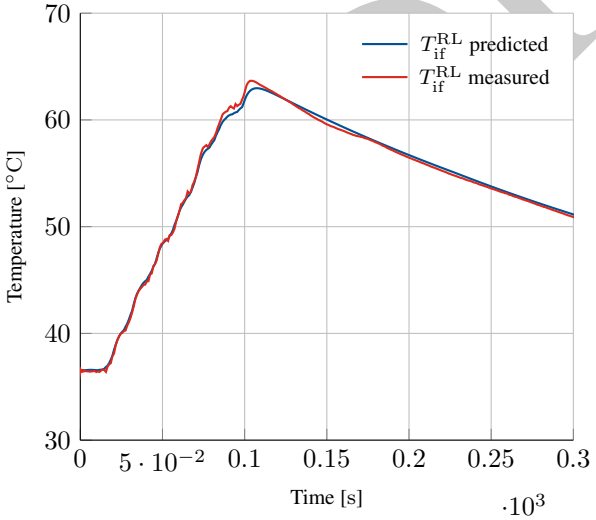

Figure 11: Comparison between predicted interface temperature and measured interface temperature for consecutive braking manoeuvre during on-road driving

Pad wear evaluation

A first limited validation for the wear model was attempted by comparing the mass of the newly installed braking pad before and after all previously presented runs. The predicted wear mass was also computed by summing the loss of mass over all the corresponding simulations (Table 2). Although a good match is observed between measured and predicted wear, further tests are required to more accurately validate this part of the simulation model.

Conclusion

In this work, a scalable model of an EV's braking system was presented with a focus on the thermal, friction and wear behaviour. An experimental setup and identification methodology were also proposed and evaluated. The

Table 2: Predicted and measured wear on a single rear-left braking pad

Parameter	$m^{\mathrm{RL}}_{\mathrm{PM}}$ [g]	$\bar{h}^{\mathrm{RL}}$ [mm]
Measured	1.7	6.5e−2
Predicted	1.5	5.9e−2
Error	11.7%	8.8%

resulting parametrised models showed a promising correlation with the experimental results. Finally, simulations on the emissions associated with brake pad wear highlighted that it is important to look not only at the emissions related to ICE, but also at those associated with braking. The resulting simulation model can be used for the sizing, design and validation of electrical and mechanical braking strategies.

Recommendations

Recommended future work includes the evaluation of the real-time capability of the simulation model. This would enable its integration in an Hardware-in-the-Loop (HiL) system to impose realistic boundary conditions for the testing of regenerative braking Electronic Control Units (ECUs), or in model-based E-motor dynamometers for instance. The simulation of the hydraulic sub-model should also be further studied in this context. Finally, further validation tests of the emission predictions should be executed.

Symbols

$A^{\mathrm{i}}_{\mathrm{pad}}$ Area of the brake pad of the i^{th} brake.

$A^{\mathrm{i}}_{\mathrm{pist}}$ Area of the brake piston of the i^{th} brake.

$C^{\mathrm{i}}_{\mathbf{j}}$ Thermal capacitance of component j of the i^{th} brake.

P_{br} Braking power.

$R^{\mathrm{i}}_{\mathbf{j}}$ Thermal resistance of component j of the i^{th} brake.

$T^{\mathrm{i}}_{\mathbf{j}}$ Temperature of component j of the i^{th} brake.

$T_{\mathbf{amb}}$ Ambient temperature.

$\bar{h}^{\mathrm{i}}$ Worn height of a single pad at the i^{th} brake.

$\bar{r}^{\mathrm{i}}$ Average braking radius of the i^{th} brake.

$\ddot{x}$ Longitudinal acceleration of the car.

$\dot{Q}^{\mathrm{i}}$ Friction heat rate generation at the pad-disk interface.

$\dot{x}$ Longitudinal speed of the car.

$\mathrm{PM}^{\mathrm{i}}_{10}$ Particle mass < 10 µm emitted by a single pad at the i^{th} brake.

$\mathrm{PM}^{\mathrm{i}}_{2.5}$ Particle mass < 2.5 µm emitted by a single pad at the i^{th} brake.

$\mathrm{i} \in \{\mathrm{RL}, \mathrm{RR}, \mathrm{FL}, \mathrm{FR}\}$ Set of brakes in the car.

μ Disk-pad friction coefficient.

ω^{i} Rotational speed of the i^{th} disk.

ρ_{pad} Density of the pad material.

τ^{i} Braking torque of the i^{th} brake.

$\mathbf{j} \in \{\mathbf{pad}, \mathbf{hub}, \mathbf{cal}, \mathbf{fluid}, \mathbf{disk}\}$ Components in a brake.

k Dimensional wear coefficient of the pad.

$m^{\mathrm{i}}_{\mathrm{PM}}$ Particle mass emitted by a single pad at the i^{th} brake.

$m^{\mathrm{i}}_{\mathrm{f}}$ Worn mass of a single pad at the i^{th} brake.

$p^{\mathrm{i}}_{\mathbf{cal}}$ Calliper pressure of the i^{th} brake.

u_b Driver brake input.

Acronyms

ECU Electronic Control Unit.

EV Eletric Vehicle.

HiL Hardware-in-the-Loop.

ICE Internal Combustion Engine.

OEM Original Equipment Manufacturer.

References

1. European Environment Agency,, *Electric vehicles from life cycle and circular economy perspectives*, 2018, doi:10.2800/77428

2. Ruan, J., Walker, P. D., Watterson, P. A., and Zhang, N., "The dynamic performance and economic benefit of a blended braking system in a multi-speed battery electric vehicle," *Applied Energy*, vol. 183, 1240 – 1258, 2016, doi:10.1016/j.apenergy.2016.09.057

3. Zhang, J., Lv, C., Gou, J., and Kong, D., "Cooperative control of regenerative braking and hydraulic braking of an electrified passenger car," *Proceedings of the Institution of Mechanical Engineers, Part D: Journal of Automobile Engineering*, vol. 226, no. 10, 1289–1302, 2012, doi:10.1177/0954407012441884

4. de Santiago, J., Bernhoff, H., Ekergård, B., Eriksson, S. *et al.*, "Electrical motor drivelines in commercial all-electric vehicles: A review," *IEEE Transactions on Vehicular Technology*, vol. 61, no. 2, 475–484, 02 2012, doi:10.1109/TVT.2011.2177873

5. Wager, G., Whale, J., and Braunl, T., "Performance evaluation of regenerative braking systems," *Proceedings of the Institution of Mechanical Engineers, Part D: Journal of Automobile Engineering*, vol. 232, no. 10, 1414–1427, 2018, doi:10.1177/0954407017728651

6. Berzi, L., Favilli, T., Locorotondo, E., Pierini, M., and Pugi, L., "Real time models of automotive mechatronics systems: Verifications on "toy models"," *IFToMM ITALY 2018: Advances in Italian Mechanism Science*, vol. 68, 141–148, 10 2018, doi:10.1007/978-3-030-03320-0_15

7. Pugi, L., Favilli, T., Berzi, L., Locorotondo, E., and Pierini, M., "Brake blending and optimal torque allocation strategies for innovative electric powertrains," *ApplePies 2018: Applications in Electronics Pervading Industry, Environment and Society*, vol. 573, 477–483, 5 2019, doi:10.1007/978-3-030-11973-7_57

8. Pugi, L., Favilli, T., Berzi, L., Locorotondo, E., and Pierini, M., "Application of regenerative braking on electric vehicles," *IEEE International Conference on Environment and Electrical Engineering and 2019 IEEE Industrial and Commercial Power Systems Europe (EEEIC / I&CPS Europe)*, 1–6, 2019, doi:10.1109/EEEIC.2019.8783318

9. Crolla, D. A. and Cao, D., "The impact of hybrid and electric powertrains on vehicle dynamics, control systems and energy regeneration," *Vehicle System Dynamics*, vol. 50, 95–109, 2012, doi:10.1080/00423114.2012.676651

10. Grigoratos, T. and Martini, G., "Brake wear particle emissions: a review," *Environmental science and pollution research international*, vol. 22, 10 2014, doi:10.1007/s11356-014-3696-8

11. Robertson, A. and Gross, D., "An electrical-analog method for transient heat-flow analysis," *Journal of Research of the National Bureau of Standards*, vol. 61, p. 105, 08 1958, doi:10.6028/jres.061.016

12. Wahlstrom, J., "A comparison of measured and simulated friction, wear, and particle emission of disc brakes," *Tribology International*, vol. 92, 503–511, 2015, doi:10.1016/j.triboint.2015.07.036

13. Andersson, S., "Wear simulation," in *Advanced Knowledge Application in Practice*, Fuerstner, I., Ed. Rijeka: IntechOpen, 2010, ch. 2, doi:10.5772/10349

14. Perricone, G., Matejka, V., Alemani, M., Valota, G. *et al.*, "A concept for reducing pm10 emissions for car brakes by 50%," *Wear*, vol. 396-397, 135 – 145, 2018, doi:10.1016/j.wear.2017.06.018

15. Garg, B. D., Cadle, S. H., Mulawa, P. A., Groblicki, P. J. *et al.*, "Brake wear particulate matter emissions," *Environmental Science & Technology*, vol. 34, no. 21, 4463–4469, 2000, doi:10.1021/es001108h

16. Kus, A., Isik, Y., Cakir, M., Coskun, S., and Ozdemir, K., "Thermocouple and infrared sensor-based measurement of temperature distribution in metal cutting," *Sensors*, vol. 15, 1274–91, 01 2014, doi:10.3390/s150101274

17. Genta, G. and Morello, L., *The Automotive Chassis: Vol. 1: Components Design*. Springer Netherlands, 2009, doi:10.1007/978-1-4020-8676-2

Acknowledgement

This project has received funding from the European Union's Horizon 2020 research and innovation program under grant agreement No 769506.

The content of this publication does not reflect the official opinion of the European Union. Responsibility for the information and views expressed therein lies entirely with the authors.